To appear in *Vehicle System Dynamics*
Vol. 00, No. 00, Month 20XX, 1–28

Vehicle System Dynamics, Volume 56, Issue 2, 2018, pp. 221-248
DOI:10.1080/00423114.2017.1371771

Effect of handling characteristics on minimum time cornering with torque vectoring

E.N. Smith[a*], E. Velenis[a], D. Tavernini[b], D. Cao[a]

[a] *Advanced Vehicle Engineering Centre, Cranfield University, UK;* [b] *Centre for Automotive Engineering, University of Surrey, UK*

(*Received 00 Month 20XX; accepted 00 Month 20XX*)

Keywords: torque vectoring, vehicle handling, electric vehicles, optimal control, yaw rate reference, minimum time

In this paper, the effect of both passive and actively-modified vehicle handling characteristics on minimum time manoeuvring for vehicles with 4-wheel torque vectoring (TV) capability is studied. First, a baseline optimal torque vectoring strategy is sought, independent of any causal control law. An optimal control problem (OCP) is initially formulated considering 4 independent wheel torque inputs, together with the steering angle rate, as the control variables. Using this formulation, the performance benefit using torque vectoring against an electric drive train with a fixed torque distribution, is demonstrated. The sensitivity of TV-controlled manoeuvre time to the passive understeer gradient of the vehicle is then studied. A second formulation of the optimal control problem is introduced where a closed-loop torque vectoring controller is incorporated into the system dynamics of the OCP. This formulation allows the effect of actively modifying a vehicle's handling characteristic via TV on its minimum time cornering performance of the vehicle to be assessed. In particular, the effect of the target understeer gradient as the key tuning parameter of the literature-standard steady-state linear single-track model yaw rate reference is analysed.

1. Introduction

Active yaw control systems for improved performance and safety have been commonplace on passenger vehicles for the past two decades [1–5]. Today, premium vehicle manufacturers are taking these systems a step further as they continuously seek ways to deliver the most enjoyable and pleasant experience for the driver. Technology currently under development allows vehicle handling to be tailored to the desires of the individual, whether the preference is for a 'fun-to-drive' characterisitic or a stable predictability. Modern all-wheel-drive electric vehicles (EVs) offer substantial opportunities for tailoring of handling through active control of yaw dynamics by over-actuation, namely torque vectoring (TV); the distribution of wheel torques between multiple wheels. TV has the potential to extend the maximum cornering force by superior use of friction availability [1, 6–8].

*Corresponding author. Email: e.smith@cranfield.ac.uk

TV systems typically consist of a yaw rate reference, a feedback controller that outputs the required yaw moment (some systems include feedforward elements [9]) converted to individual wheel torque demands by the Control Allocator (CA). Advanced techniques using mathematical analysis and simulation tools have been used to optimise both controller [10–12] and CA performance [9, 12, 13]. In particular, de Castro et. al. [13] developed a realisable causal feedforward CA scheme, considering an electric vehicle with four independent electric motors, seeking to minimise time to navigate a U-turn bend. They achieved this by using nonlinear optimal control techniques, which permitted both the ability to gain insight into optimal controls for distribution of torques but also the realistic emulation of a racing driver. Numerous other vehicle dynamics studies using the optimal control technique to manoeuvre vehicles at the performance limit has permitted a realistic emulation of both circuit racing drivers [14–18], and rally trailbraking [19, 20]; EV-specific topologies were considered in [13, 21, 22]. The nonlinear optimal control solution gives an ideal driver behaviour (no mistakes, friction-limit operation, full preview of future conditions)–which is not possible with a causal driver model, racing-line following [16], or model predictive control.

With modern actively-controlled vehicles, the optimal control technique has been extended to not only correctly mimic the professional driver, but to gain insight into how to maximise the performance of active systems given a certain objective. Tremlett et. al. [23] explore optimum differential set-up for touring car racing, while [17] simultaneously determine optimal deployment of the complex hybrid power technology and numerous set-up options available on modern Formula 1 cars. These studies are examples of an open-loop control *method* [24, 25] from which the maximum performance potential of the vehicle with TV may be ascertained– by determining the optimal control inputs that must be applied to the vehicle *directly*. However, optimal open-loop control is a-causal and hence gives only theoretical insight; a causal control system (closed-loop control *algorithm* [24, 25]) is required to make use of the insight in a practical application.

In this work we propose the application of nonlinear optimal control techniques to study the effect of handling characteristics, passive and actively modified, of torque-vectored vehicles for minimum time manoeuvring. In [21] we generated a particular minimum time open-loop control trajectory over a U-turn for a 7 degree of freedom (DOF) vehicle model with nonlinear tyres and TV via 4 independent motors. The open-loop optimal control problem was formulated with 4 independent wheel torques and front steering rate (corresponding to the driver steering input) as the control inputs. In this paper we extend the open-loop OCP formulation of [21] to study the effect of passive handling balance, determined by the front/rear tyre characteristics, on the controlled performance.

Furthermore, the open-loop control solution generates a baseline performance as a benchmark against which a closed-loop control law is assessed. The OCP is reformulated with two control inputs of total longitudinal torque demand (corresponding to the driver's throttle/brake command) and steering rate. A closed-loop TV controller actively modifying the vehicle's handling characteristic is included in the system dynamics of the OCP. For an Unmanned Aerial Vehicle, Levin et. al. [26] produced optimal state trajectories in OCP, which were then used as reference signals to be followed in an OCP formulation including a motion controller. A framework that included the closed-loop TV controller in the system dynamics for a ground vehicle was first introduced in [22], using, however, a rather simple 3DOF single track vehicle model, with a linear tyre model and neglecting important load transfer effects, while the torque vectoring control action was applied as an external yaw moment. In this work we extend the approach of [22] by considering the 7DOF model with nonlinear tyre characteristics and load transfer effects of [21]. Torque vectoring is now realistically implemented through control of trac-

tion/braking forces at each of the 4 wheels independently. This formulation allows us to assess the effect of actively modifying the handling balance of the vehicle on minimum time cornering performance. Several approaches in the literature propose heuristic target handling characteristics for TV controlled vehicles. For instance, De Novellis et. al. [9] choose a target to produce a more agile response by reducing understeer with respect to the passive vehicle. Our analysis investigates the sensitivity of manoeuvre time to the target handling characteristic with the purpose of informing engineers how to optimise the performance of a TV vehicle.

2. Vehicle System Modelling

This section sets out the mathematical models required for the optimal control problem formulation in §3.

2.1. *7DOF Vehicle Model*

A 7DOF, two-track vehicle model is employed with nonlinear tyres (Fig. 1), including a quasi-static representation of longitudinal and lateral load transfers. Roll and pitch dynamics are neglected. Retarding torque is provided exclusively by regenerative braking. In a similar manner to [19, 20], aerodynamic forces and rolling resistance are neglected since the manoeuvre under consideration is of moderate speed. The equations are parameterised for a high-performance EV (Table 1). In the following, $i = \{F, R\}$ (front, right), $j = \{L, R\}$ (left, right), $k = \{x, y, z\}$. x, y and z denote the longitudinal, lateral and vertical directions respectively. Quantities without subscript k denote resultants. The

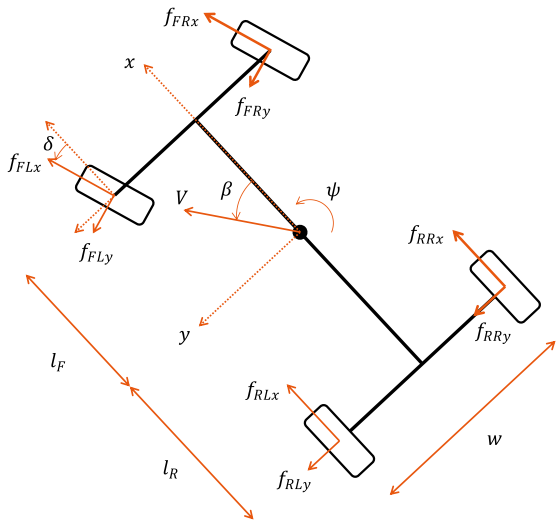

Figure 1.: 7DOF vehicle model

equations of motion for the 7DOF vehicle model (Fig. 1) are:

$$\dot{V} = \frac{1}{m}\left[(f_{FLx} + f_{FRx})\cos(\delta - \beta) - (f_{FLy} + f_{FRy})\sin(\delta - \beta)\right. \tag{1}$$
$$\left. + (f_{RLx} + f_{RRx})\cos\beta + (f_{RLy} + f_{RRy})\sin\beta\right],$$
$$\dot{\beta} = \frac{1}{mV}\left[(f_{FLx} + f_{FRx})\sin(\delta - \beta) + (f_{FLy} + f_{FRy})\cos(\delta - \beta)\right. \tag{2}$$
$$\left. - (f_{RLx} + f_{RRx})\sin\beta + (f_{RLy} + f_{RRy})\cos\beta\right] - \dot{\psi},$$
$$\ddot{\psi} = \frac{1}{I_z}\left[\ell_F\left\{(f_{FLy} + f_{FRy})\cos\delta + (f_{FLx} + f_{FRx})\sin\delta\right\} - \ell_R\,(f_{RLy} + f_{RRy})\right. \tag{3}$$
$$+ w/2\,(f_{FLy}\sin\delta - f_{FLx}\cos\delta - f_{RLx})$$
$$\left. + \; w/2\,(f_{FRx}\cos\delta - f_{FRy}\sin\delta + f_{RRx})\right]$$
$$\dot{\omega}_{ij} = \frac{1}{I_w}\left[T_{ij} - f_{ijx}r\right], \tag{4}$$

where: m is the vehicle mass; I_z is the moment of inertia about the vertical axis; V is the vehicle velocity at the center of mass (CM); β is the vehicle sideslip angle at the CM; $\dot{\psi}$ is the yaw-rate. The moment of inertia of each wheel about its axis of rotation is I_w; the wheel radius is r; the wheel angular speeds are ω_{ij}; the steering angle is δ; the drive/brake torque applied on each wheel is T_{ij}. Tyre forces are denoted by f_{ijk}. The parameters ℓ_F, ℓ_R determine the location of the CM with respect to the center of each wheel; w is the track width.

The tyres are modelled using the simplified Pacejka Magic Formula (MF) [27], assuming tyre friction force is linearly dependent on the tyre normal force, and isotropic tyre force characteristics:

$$\mu_{ij}(|s_{ij}|) = \mathrm{MF}(|s_{ij}|) = D\sin(C\mathrm{atan}(B_i s_{ij})), \quad \text{where: } |s_{ij}| = \sqrt{s_{ijx}^2 + s_{ijy}^2}, \tag{5}$$

where $|s_{ij}|$ is the resultant tyre slip magnitude, and s_{ijx} and s_{ijy} are the theoretical longitudinal and lateral slips, respectively [27]; μ_{ij} is the total tyre force coefficient; B_i, C, D are the MF coefficients. Tyre force components are given by:

$$|f_{ij}| = \sqrt{f_{ijx}^2 + f_{ijy}^2}, \quad \text{where: } f_{ijk}/f_{ijz} = \mu_{ijk} = -\frac{s_{ijk}}{|s_{ij}|}\mu_{ij}(|s_{ij}|), \tag{6}$$

where μ_{ijk} are the tyre force coefficients for tyre ij in longitudinal or lateral directions ($k = \{x, y\}$). Similarly, s_{ijk} is the theoretical slip quantity for tyre ij in the $k = \{x, y\}$ directions.

A quasi-static representation is used to determine the normal loads on each wheel, f_{ijz}, adopted from [28] and re-presented here, by neglecting pitch, roll and vertical translation—considering only the static weight distribution and weight transfers generated by lateral and longitudinal accelerations. The normal loads on each wheel are given by:

$$f_{FLz} = f_{FLz}^0 - \Delta f_L^x - \Delta f_F^y, \qquad f_{FRz} = f_{FRz}^0 - \Delta f_R^x + \Delta f_F^y, \tag{7}$$
$$f_{RLz} = f_{RLz}^0 + \Delta f_L^x - \Delta f_R^y, \qquad f_{RRz} = f_{RRz}^0 + \Delta f_R^x + \Delta f_R^y,$$

Table 1.: Vehicle and tyre model parameters, and manoeuvre boundary conditions

(a) Vehicle Parameters

Symbol	Name	Unit	Value
m	mass	kg	1137
L	wheelbase	m	2.5
w	track width	m	1.374
h	height of CM	m	0.317
ℓ_f	distance of CM to front axle	m	1.187
ℓ_r	distance of CM to rear axle	m	1.313
I_z	yaw moment of inertia	kgm^2	1174
μ_{max}	tyre-road friction coefficient	-	1
r	wheel radius	m	0.298
n_δ	rack ratio	-	16
B_f	front Pacejka stiffness factor[a]	-	16.4
B_r	rear Pacejka stiffness factor[a]	-	20.7
C	Pacejka shape factor	-	1.46
D	Pacejka peak factor	-	1
T_{max}	motor torque limit	Nm	800
P_{max}	motor power limit	kW	90

(b) Boundary Conditions

$\mathbf{x}$	$\mathbf{x}_0$	$\mathbf{x}_f$
s	0	s_f
V	free[b]	free
$\dot{\psi}$	0	free
ω_{ij}	free	free
s_n	free	free
χ	0	free
x_R	free	free
y_R	free	free
$\frac{\pi}{2}$	free	free
δ	0	free
t	0	free

(c) Tyre parameters for passive steady-state understeer gradient set-up

Parameter	Unit	Values				
Passive understeer gradient, K^{SS}_{pas}	°/g	-1.0	-0.5	0.0	0.5[a]	1.0
Front tyre cornering coefficient, η_f	rad^{-1}	24	24	24	24	24
Rear tyre cornering coefficient, η_r	rad^{-1}	17	20	24	30	41
Front Pacejka stiffness factor, B_f	-	16.4	16.4	16.4	16.4	16.4
Rear Pacejka stiffness factor, B_r	-	11.7	13.6	16.4	20.7	28.0

[a]baseline passive steady-state understeer gradient; [b]'free' within state/constraint bounds

where the static normal loads are:

$$f^0_{FLz} = f^0_{FRz} = \frac{mg\ell_R}{2(\ell_F+\ell_R)}, \qquad (8)$$
$$f^0_{RLz} = f^0_{RRz} = \frac{mg\ell_F}{2(\ell_F+\ell_R)}.$$

Changes in normal load arising due to lateral acceleration across the front and rear axles are given by:

$$\Delta f^y_F = \frac{mh\ell_R}{w(\ell_F+\ell_R)}a_y, \qquad \Delta f^y_R = \frac{mh\ell_F}{w(\ell_F+\ell_R)}a_y, \qquad (9)$$

while the changes due to longitudinal acceleration on the left and right tracks are given

by:

$$\Delta f_L^x = \Delta f_R^x = \frac{mh\ell_R}{2(\ell_F + \ell_R)} a_x. \tag{10}$$

The passive, steady-state understeer gradient of the vehicle is defined as [29]:

$$K_{pas}^{SS} = \left(\frac{1}{\eta_f} - \frac{1}{\eta_r} \right) / g. \tag{11}$$

The passive vehicle's understeer gradient is modified by selecting cornering coefficient values η_f and η_r, assuming that the cornering coefficient is constant, where:

$$\eta_f = B_f CD \qquad \eta_r = B_r CD. \tag{12}$$

Equation (11) is valid considering the small angle assumption. In [30], ranges are given for where the trigonometric functions remain valid; both slip angles and steering angles in the following results do not exceed 10°, hence the approximation holds well.

2.2. *Road model*

In the following, a U-turn manoeuvre consisting of two 50m straights joined by a bend of constant radius of curvature, with turn radius, R, is considered, as shown in Figure 4.

3. Optimal Control Formulations

This section describes the optimal control problems (OCP), the corresponding mathematical formulation and numerical optimisation solver to be used in the open- and closed-loop analyses.

3.1. *Control configurations*

To meet the objectives of generating baseline optimal trajectories, assessing passive charactistics on controlled behaviour, and to evaluate the effect of modifying the yaw rate reference of the TV controller, two OCP formulations are required. Figure 2(a) shows the open-loop *control method* [24, 25] from which the maximum performance potential of the vehicle with TV may be ascertained– by determining the optimal control inputs that must be applied to the vehicle *directly*. The efficient cause[1] of this control is a 'perfect', 'super-human' driver. 'Perfect', is defined as 'the ability to operate the vehicle at the limit of adhesion at every instant without making errors'. 'Super-human' meaning he has direct authority over individual wheel torques (T_{ij} in (21)). This formulation is used to generate the baseline optimal trajectories for TV in §4.1, and to analyse the effect of passive handling balance on controlled response in §4.2.

Figure 2(b) shows the closed-loop *control algorithm* formulation [24, 25]. Perfect open-loop control is a-causal and hence only of theoretical interest; a causal active yaw control system is required to determine the torques applied at each wheel to follow the desired

[1] Aristotle. Physics, 195a

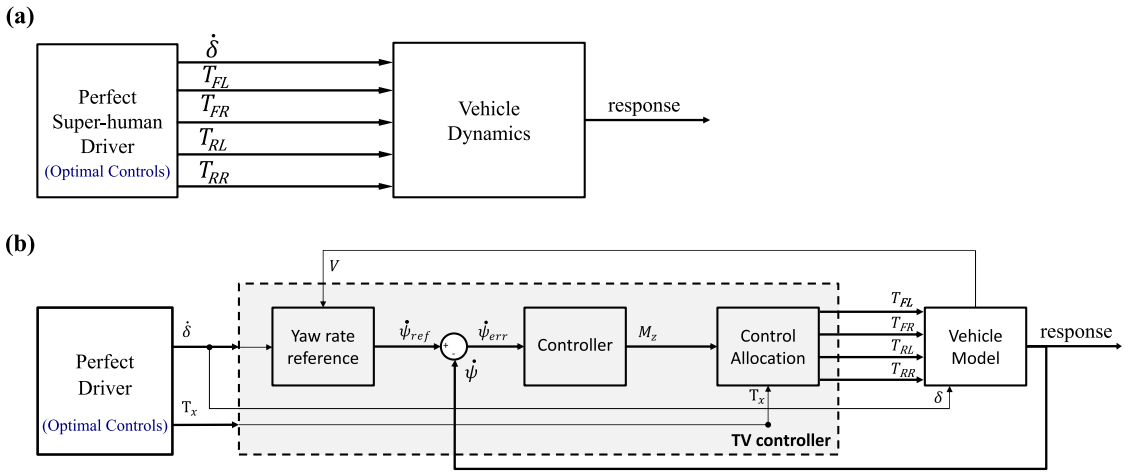

Figure 2.: In the open-loop OCP formulation (a), the control inputs are steering rate and 4 torques. In the closed-loop OCP (b), the control inputs to be optimised are steering rate and torque demand. The 4 wheel torques are determined by the closed-loop TV controller which follows a yaw rate reference corresponding to the desired modified handling behaviour.

high-level motion objectives– in this case yaw rate, $\dot{\psi}$, and total longitudinal torque demand, T_x. The specific component of interest for this research is the yaw rate reference, and by incorporating a closed-loop controller into the system dynamics of the OCP, the performance of the reference may be evaluated (§5). To evaluate the reference, a 'perfect' driver is once again required but, in this instance, merely a 'human' one, with authority over only longitudinal torque demand and steering (equation 22), not individual wheel torques which are now outputs of the control allocation. Further detail is given in §5.

3.2. *Mathematical Formulation*

To find the optimal controls and corresponding vehicle states required to achieve a specified manoeuvre in minimum time, optimal control problems are mathematically formulated as follows. Consider a dynamic system in the general state-space form:

$$\dot{\mathbf{x}} = \mathbf{f}[\mathbf{x}(t), \mathbf{u}(t)], \tag{13}$$

where $\mathbf{x}$ and $\mathbf{u}$ are state and control vectors respectively and t is the elapsed time.

Although the objective is to minimise time, a change of the independent variable is now performed. Elapsed time, t, is transformed to distance travelled along the road centreline, s, such that the formulation must now be expressed with respect to s (see Figure 3). Two related coordinates are required to map differential equations from time to distance: lateral position relative to the road centreline, s_n, and the angle of the vehicle relative to the road centreline, χ [17, 31]. This change of coordinate reference frame, from vehicle-centred to road-centred 'curvilinear coordinates', is made to ensure affine road boundary constraints.

Thus the dynamic system in (13) becomes:

$$\dot{\mathbf{x}}(\mathbf{s}) = \mathbf{f}[\mathbf{x}(s), \mathbf{u}(s)]; \tag{14}$$

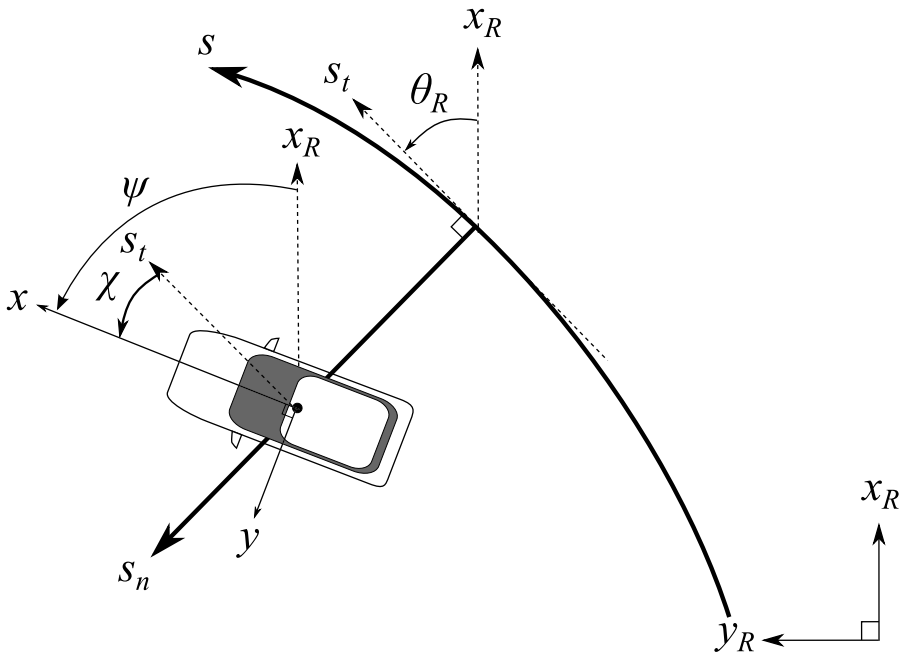

Figure 3.: Curvilinear coordinate definition; independent variable, s, distance travelled along road centreline

The OCP now seeks to find the control vector sequence to minimise the cost function:

$$J = \phi[\mathbf{x}(s_0, s_f)] + \int_{s_0}^{s_f} L[\mathbf{x}(s), \mathbf{u}(s)], \tag{15}$$

subject to initial and final conditions:

$$\mathbf{x}(s_0) = \mathbf{x}_0, \qquad \mathbf{x}(s_f) = \mathbf{x}_f, \tag{16}$$

and equality and inequality constraints:

$$\mathbf{p}[\mathbf{x}(s), \mathbf{u}(s)] = 0, \qquad \mathbf{g}[\mathbf{x}(s), \mathbf{u}(s)] \leq 0, \tag{17}$$

where 0 and f subscripts denote initial and final values, ϕ denotes the Mayer term and L denotes the Lagrange integral term.

The curvilinear coordinate frame is shown in Figure 3, and time derivatives are defined as:

$$\dot{s} = \frac{(V_x cos\chi - V_y sin\chi)}{1 - s_n \kappa_R}, \qquad \dot{s}_n = V_x sin\chi - V_y cos\chi, \qquad \dot{\chi} = \dot{\psi} - \kappa_R \dot{s}, \tag{18}$$

$$\text{where } V_x = V cos\beta, \qquad V_y = V sin\beta, \tag{19}$$

and V is the vehicle speed, κ_R is the instantaneous path curvature of the road centreline, $\dot{\psi}$ is the vehicle yaw rate and β is the sideslip angle at the CM. In Figure 3, s_t, denotes the tangent to the road centreline at point s. The state and control vectors for the vehicle

model configurations are:

$$\mathbf{x}(s) = \{V(s), \beta(s), \dot{\psi}(s), \omega_{ij}(s), x_R(s), y_R(s), \theta_R(s), s_n(s), \chi(s), \delta(s), t(s)\}^T, \quad (20)$$

$$\mathbf{u}(s) = \{T_{FL}(s), T_{FR}(s), T_{RL}(s), T_{RR}(s), \dot{\delta}(s)\}^T, \quad (21)$$

where T_{ij} are the individual wheel torques, $\dot{\delta}$ is steering rate. Time elapsed, t, is included as a state to allow analysis as a function of time to be performed. For the *closed-loop control method* (TV), the control vector includes only overall torque demand, T_x (as illustrated in Figure 2(b)):

$$\mathbf{u}(s) = \{T_x(s), \dot{\delta}(s)\}^T. \quad (22)$$

Equations of motion (1-4) and curvilinear coordinates (18) are transformed from a time-base to a distance-base as follows:

$$\frac{d\zeta}{ds} = \zeta' = \frac{d\zeta}{dt}\frac{dt}{ds} = \dot{\zeta}\dot{s}^{-1} \quad (23)$$

where ζ is any state. Control-related state distance derivatives, δ and t, are calculated:

$$\frac{d\delta}{ds} = \delta' = \frac{\delta}{dt}\frac{dt}{ds} = \dot{\delta}\dot{s}^{-1}, \quad (24)$$

$$\frac{dt}{ds} = t' = \dot{s}^{-1}. \quad (25)$$

Distance derivatives of the global coordinates of the road centreline are given as:

$$x'_R = \cos\theta_R, \qquad y'_R = \sin\theta_R, \qquad \theta'_R = \kappa_R, \quad (26)$$

where x_R, y_R are the global coordinates on two nominal orthogonal axes relative to an origin and θ_R is the heading relative to that origin.

In the current study, the cost function is composed primarily of the Lagrange integral term to minimise time to complete the manoeuvre. The Mayer term is introduced to ensure straight-line running conditions at the start of the manoeuvre. The cost function is:

$$J(s) = W_0\phi[\mathbf{x}(s_0, s_f)] + \int_{s_0}^{s_f} \frac{1}{\dot{s}}\, ds, \qquad \text{where} \quad (27)$$

$$\phi[\mathbf{x}(s_0, s_f)] = \frac{\beta_0^2}{\bar{\beta}^2} + \frac{\dot{\psi}_0^2}{\bar{\dot{\psi}}^2} + \frac{\delta_0^2}{\bar{\delta}^2} + \frac{\chi_0^2}{\bar{\chi}^2}, \quad (28)$$

where β_0, $\dot{\psi}_0$, δ_0 and χ_0 are initial sideslip, yaw rate, steer angle and relative yaw angle values respectively. '$\bar{\mathbf{x}}$' are normalisation factors for the equivalent states. W_0 is the relative weighting of the Mayer term for the initial conditions. The full set of boundary conditions are tabulated in Table 1. Including the initial conditions in the cost function is more tractable for the solver than imposing a hard constraint.

For optimisation considering the uncontrolled vehicle, a static torque distribution is enforced by including an additional term into the Lagrange integral expression. Again,

considering torque limits in the cost function is more tractable than setting torque limits as a hard constraint:

$$J(s) = W_0\phi[\mathbf{x}] + \int_{s_0}^{s_f} \left(\frac{\dot{s}^{-1}}{\bar{t}} + W_T \frac{(T_{FL}-T_{FR})^2+(T_{RL}-T_{RR})^2+(T_{FL}(1-\gamma)-\gamma T_{RL})^2}{\bar{T}^2} \right) ds, \tag{29}$$

where $\bar{t}$ and $\bar{T}$ are time- and torque-normalisation factors respectively, W_T is the relative weighting on the torque terms and γ is the proportion of total torque applied at the front axle.

It is assumed that the driver is capable of instantaneously switching between accelerator and brake. In addition to road boundary constraints, steering rate bandwidth is limited to 1Hz [32, 33]:

$$|\dot{\delta}| \leq \dot{\delta}_{max}, \qquad |T_{ij}| \leq T_{max}, \tag{30}$$

where δ_{max} denotes the maximum steering rate and T_{max} denotes the maximum torque of each individual motor. Finally, road boundary constraints are expressed:

$$w_{R,l} \leq s_n \leq w_{R,r}, \tag{31}$$

where $w_{R,l}$ and $w_{R,r}$ denote the left and right road widths.

3.3. *Solver*

$GPOPS-II$ [34] is used to solve the optimal control problems, which transcribes the continuous-time OCP into a discrete nonlinear programming problem (NLP) using the Legendre-Gauss-Radau quadrature orthogonal collocation approach. *ADIgator* [35] automatic differentiation software is used to calculate derivatives. Simulations were performed on a desktop PC with 8GB RAM and an Intel® Core^{TM} i7-3370 CPU at 3.40GHz delivering a computation time between 3 and 60 minutes depending on the particular OCP setup.

Remark 1 The optimal control problem must be preconditioned to improve the performance of the optimisation algorithm [36]. Decision variables must be as equally-weighted as possible to minimise errors in determination of the search direction to improve rate of convergence. Scaling the state matrix to improve conditioning is performed to ensure all decision variables are $\mathcal{O}(1)$. A scaling scheme has been applied in the same manner as [37], achieved by applying scaling factors to all physical quantities, based on three fundamental quantities of length, mass and time. For example: let mass scaling factor $\tilde{m} = m^{-1}$, then scaled mass becomes $m\tilde{m} = 1$; let length scaling factor $\tilde{L} = L^{-1}$, then scaled wheelbase becomes $L\tilde{L} = 1$; let time scaling factor $\tilde{t} = \sqrt{(L/g)}$, then scaled time becomes $t\tilde{t}$. Velocity is scaled by a combination of length and time scaling factors, according to its units, and becomes $V\tilde{L}\tilde{t}^{-1}$. The conditioned dual problem is solved and then unscaled to give results in the original domain. To improve performance further, non-smooth operations such as *min*, *max*, *sign* and *abs* have been replaced by close approximations that are continuously differentiable [37].

4. Open-loop control method

In this section, the absolute potential of the TV system is determined. This is the *open-loop control method* described in §3.1 (Fig. 2(a)). This will allow the torque vectoring performance to be compared against the uncontrolled vehicle in §4.1. It will also allow analysis of what effect the passive, steady-state understeer gradient has on the controlled response in §4.2.

A U-turn manoeuvre (Figure 4) with $R = 35$m is navigated. In general terms, the vehicle enters the manoeuvre on the right at high speed in a straight line, exerting maximum braking torque. As the speed reduces and the road curvature increases, braking is reduced, steering is gradually applied until the maximum curvature point is reached and the vehicle has moved to the inside road boundary. After this midpoint (where lateral acceleration is maximal), torque is gradually applied, steering is reduced to zero as high-speed, straight-line running is approached and the vehicle returns to the outside road boundary.

4.1. *Uncontrolled vs. Torque Vectoring*

The optimal control problems for uncontrolled and TV-controlled vehicle set-ups are presented for comparison in this section. The TV set-up is formulated as in §3, with cost function (27). The uncontrolled vehicle (hereafter, *Unctrl*) is compared by setting the static drive torque distribution to produce 4WD, ($\gamma_{drive} = 0.6$). Braking distribution is $\gamma_{brake} = 0.7$. These distributions require cost function (29). Finally, the impact of TV with dynamic load transfer (LT) removed (i.e. normal loads become simply a function of static weight distribution) is examined (hereafter *Unctrl no LT*).

Thus three open-loop control method optimisations are now presented for comparison. With torque vectoring capability, the manoeuvre time of 8.502s is 0.380s (to 3 significant figures) faster than *Unctrl*. This is a significant benefit for just one corner and, when extrapolated over a whole lap of 10-15 turns, would give a benefit of the order of $\sim 3-4$s, which is considerable in the racing context. *TV no LT* is 0.038s faster than TV: In this analysis, two plots will be examined.

First, Figure 5 overlays states, controls and calculated quantities for all optimisations. A dynamic scenario is considered, yet the steady-state understeer gradient calculated at every instant is still useful in giving an indication of vehicle handling behaviour, defined as follows [29]:

$$K_{inst}^{SS} = \frac{\frac{V\delta}{\psi} - L}{V^2}. \tag{32}$$

K_{inst}^{SS} is plotted in Figure 5(d). Further insight is drawn from plots of friction utilisation, as shown in Figure 6, for each tyre separately. Friction utilisation is defined as the lateral, longitudinal or resultant force divided by the total force available on the wheel:

$$\mu_{ijk} = \frac{F_{ijk}}{\mu_{max} F_{ijz}}, \tag{33}$$

where $i \in [F, R]$; $j \in [L, R]$; $k \in [x, y]$ and μ_{max} is the tyre-road friction coefficient.

Subfigures enumerated with (i) show friction utilisation on the friction circle; subfigures enumerated with (ii) show friction utilisation as a function of distance travelled (lateral

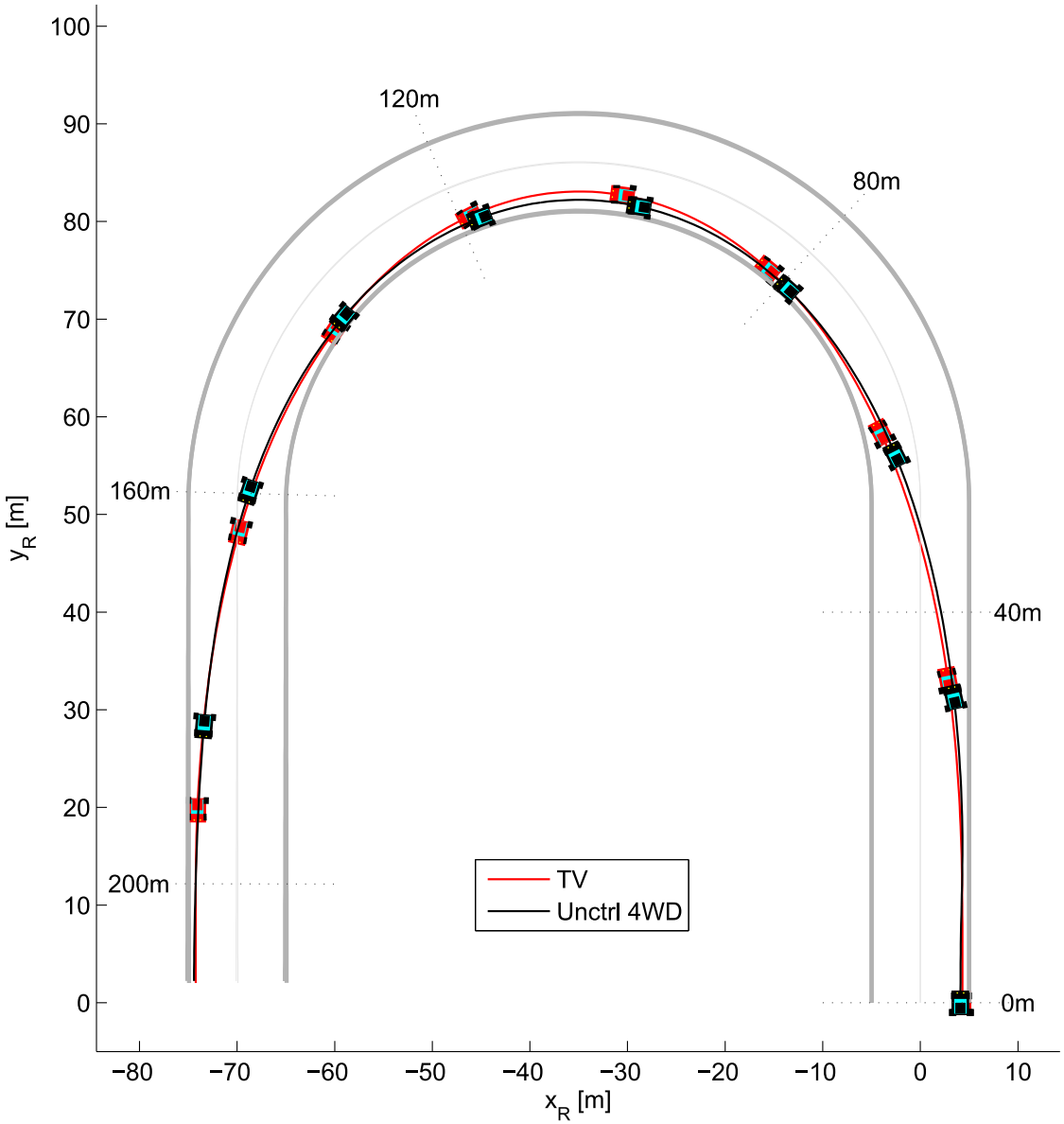

Figure 4.: Comparison of path trajectories for torque vectoring and the uncontrolled vehicle with 70:30 front:rear static brake torque distribution and 60:40 propulsive torque distribution. Vehicle position is plotted every second.

and total). Accelerations at the centre of gravity (CM) are shown in subfigures (e.i) and (e.ii) in a similar manner (lateral, longitudinal and total).

Looking first of all at the vector velocity and acceleration traces, with reference to Figure 5(a) and 6(f), it is clear that TV is able to sustain a greater magnitude of total longitudinal acceleration and hence can both start and exit the manoeuvre at higher speeds than *Unctrl*.

There is an interesting difference in path trajectory at the midpoint (Fig. 4): the uncontrolled vehicle takes a tighter line, hugging the inside edge of the track for $80 < s < 130$m, whilst TV takes more of a 'double apex', reaching a point of maximum path curvature ($\max(\kappa_{path})$, at point of minimum speed, V_{min}) at $s = 0.5s_f$. TV has a lower V_{min}, since, in effect, its maximum path curvature is greater than the uncontrolled paths:

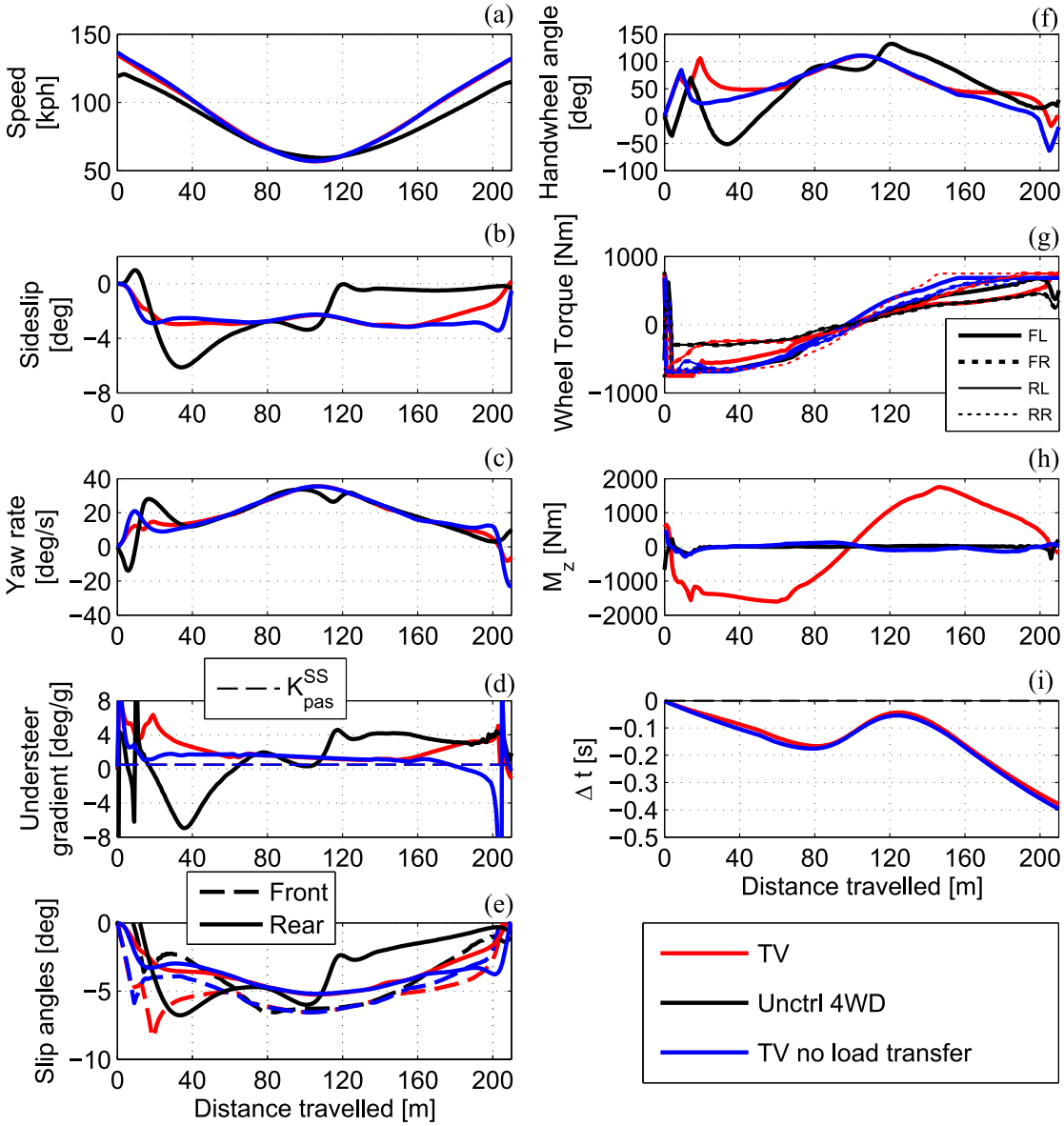

Figure 5.: Comparison of torque vectoring with uncontrolled vehicle, and for torque vectoring when load transfer effects are neglected: states and controls

$V_{min} \approx \sqrt{\frac{a_{centripetal}}{\max(\kappa_{path})}}$. The uncontrolled vehicle is able to maintain 3km/h higher speed over $90 < s < 120$m and thus gain time back during this portion of the manoeuvre.

TV uses all friction available on each wheel through most of the manoeuvre. When torques are saturated by motor limits, a small reduction in friction utilisation is observed at the front tyres during high-speed deceleration ($0 < s < 40$m) and on the rear tyres at high-speed acceleration ($180 < s < 210$m). The torque limits reduce the amount of torque vectoring that can be applied at high speed (Figure 5(h)) and, therefore, greater handwheel angle (Figure 5(f)) is required to compensate for the reduced influence on the lateral dynamics that are possible from the both the left-right torque difference and the coupling effect of longitudinal forces on lateral forces via the friction circle. The handwheel angle increases the understeer gradient during these periods (Figure 5(d)).

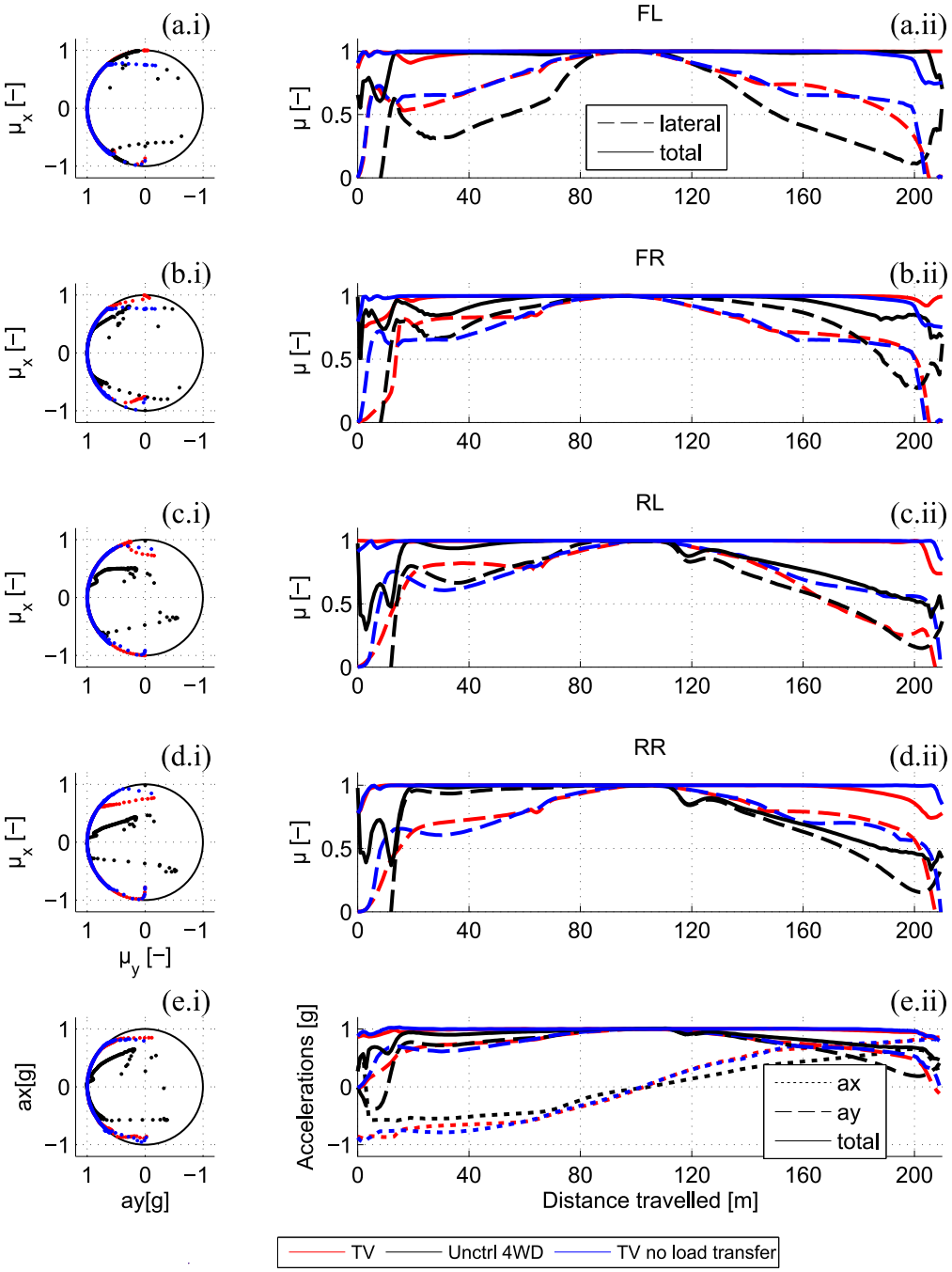

Figure 6.: Comparison of torque vectoring with uncontrolled vehicle, and for torque vectoring when load transfer effects are neglected: friction utilisation

TV is highly understeering during turn entry (where yaw moment is stabilising) and maintains a near-constant understeer gradient for most of the turn before increasing once again as torques reach their limits. *Unctrl* exhibits high levels of oversteer for turn-entry during the pendulum turn, progressing to mild understeer at the apex, with significant levels of understeer over the second half of the manoeuvre during acceleration. Oversteer during turn entry is due to use of the pendulum-turn technique (yawing out of the turn before yawing into the turn).

Friction usage for *Unctrl* is maximal for FL for the duration of the manoeuvre. FR friction is ~ 0.8 during high speed portions. During braking, rear tyres usage is near-unity but during acceleration, front tyre use reduces to only ~ 0.5 at the end of the manoeuvre. This is due to a torque distribution that favours the less-loaded front tyres, despite the rearward load transfer that occurs during acceleration.

Figure 5(d) shows that *TV* is able to 'flatten' the understeer gradient characteristic substantially when compared with *Unctrl*, through applying a stabilising yaw moment during braking and a destabilising yaw moment during acceleration. This is attributed to compensation for load transfer effects. Inspection of Figure 5(h) shows that magnitude of yaw moment is proportional to a_x. This trend of direct yaw control effecting a stabilising yaw moment under deceleration and a destabilising yaw moment during acceleration is confirmed by findings for a similar electric vehicle topology analysed in [13], and a brake torque vectoring differential study for a RWD conventionally-powered touring car in research by Tremlett et. al. [18, 23, 38] and Kaspar et. al. [39]. De Novellis et. al. [9] describe a similar finding for this yaw moment trend when a yaw rate reference independent of longitudinal acceleration is used. Indeed, the β-method described in the seminal work of Shibahata et. al. [1] showed that direct yaw control can overcome load transfer effects, considering a 6DOF vehicle model with roll and pitch DOFs and nonlinear tyres.

By removing load transfer effects, further insights may be gained. For *TV no LT* (normal loads are equal to their static values according to weight distribution) almost no yaw moment is required to match the handwheel, sideslip, yaw rate and understeer gradient profiles as required by *TV*, and friction usage is near-maximal (where the vehicle is not torque-limited). This gives further credence to the theory that TV improves performance by making use of tyre force coupling effects: controlling longitudinal forces such that lateral forces are reduced/increased on each corner for a greater resultant force, and hence a greater total acceleration than would otherwise be possible.

4.2. *Effect of passive handling characteristic*

It has been demonstrated that *TV* is 0.380s faster than *Unctrl*, for a passive steady-state understeer gradient $K_{pas}^{SS} = 0.5^\circ/\text{g}$.

Since TV extends the performance envelope of the vehicle by the correct distribution of tyre forces, the pertinent question is whether there is a certain K_{pas}^{SS} for which tyre force distribution by TV gives the greatest performance envelope and therefore delivers a faster manoeuvre time. To answer this question, optimal control problems (with TV active) are formulated and solved for a range of passive understeer characteristics. This is achieved by modifying tyre parameters.

Subsequent work by the authors [22] considered the same manoeuvre for a 3DOF vehicle model with TV, with $K_{pas}^{SS} = 0.5^\circ/\text{g}$. The instantaneous understeer gradient followed the passive value very closely.

In the present study, optimisations were run for TV for $K_{pas}^{SS} = \{-1, -0.5, 0, 0.5, 1\}$ by altering front and rear tyre stiffness parameters, B_F and B_R, according to Table 1 (recall (11) and (12)). The manouevre time for all optimisations is 8.52s (to two decimal places). This clearly demonstrates that the controlled performance is insensitive to the passive characteristic of the vehicle for these modest perturbations from neutral steer, as was found for the 3DOF model results in [22].

Figure 7 shows states, controls and calculated quantities for the range of passive handling balances. Figure 7(d) shows that K_{inst}^{SS} follows K_{pas}^{SS} fairly closely for neutral steer for $60 < s < 140$m where torques are below their limit value. There is some variation with acceleration and associated normal load (as was found in [21]). Similar profiles of

understeer gradient with distance travelled are observed for all permutations: slightly greater understeer effect for $0 < s < 100$m during braking and slight reduction on understeer effect for $100 < s < 200$m during acceleration. (This is the opposite trend to that experienced by the uncontrolled vehicle). For variation in K^{SS}_{pas}, it is clear that the further from neutral steer, the greater the instantaneous understeer gradient deviates from the passive value. For example, where $K^{SS}_{pas} = 1°/\text{g}$ (red), K^{SS}_{inst} is around $\sim 3°/\text{g}$.

Where wheel torques are saturated, the understeer gradient is dramatically increased due to the greater contribution of steering required to generate the lateral forces, since torque vectoring is no longer able to assist to the same degree in the optimal redistribution of tyre forces.

Remark 2 Wheel torques (and consequently M_z) show little variation. This is an important result since it demonstrates that the control yaw moment (vehicle authority) is predominantly used to counteract load transfer effects. The main differentiator between the optimisation controls is the handwheel angle, which is increased in proportion with passive understeer gradient. Correspondingly, for sideslip angle, there is a clear trend of increasing tail-out sideslip as K^{SS}_{pas} progresses from $+1.0$ to $-1.0°/\text{g}$ (Fig. 7(c)). Steering angle (driver control authority), is used to generate front lateral force and hence the angle required depends on the understeer gradient.

Figure 8 shows friction utilisation and CM vehicle accelerations. Total friction usage for each tyre is similar in all cases (Fig. 8(a-d)). Friction use on the front tyres during $0 < s < 40$m shows a reduction from the maximum, corresponding to the curtailment of torque vectoring ability by actuator limitations. The same is true for the RR tyre when $160 < s < 210$m.

Time deltas relative to neutral steer (Figure 7(i)) show interesting symmetry about the point $s = 0.5s_f$, but no consistent trends as a function of understeer gradient. The final time deltas are of a small enough magnitude to be inconclusive, possibly as a result of optimisation peculiarities rather than the fundamental system dynamics.

In summary, for the 7DOF, as for the 3DOF model in [22], manoeuvre time for the controlled vehicle is insensitive to the passive vehicle understeer characteristic for this manoeuvre. For the 3DOF model, the controlled understeer gradient follows the passive value closely; for the 7DOF model, controlled understeer gradient deviates increasingly from the passive value the further away from neutral steer. In addition, the 7DOF understeer gradient is not constant for the manoeuvre but shows a small variation towards greater understeer during deceleration and vice versa for acceleration, and a significant increase where torque vectoring is limited by motor constraints.

It must be reiterated that the open-loop set-up with T_{ij} directly applied is unrealisable in the real world for reasons noted in §3.1; nonetheless it demonstrates the open-loop optimal controls required to achieve optimality in terms of time minimisation. The next section will evaluate how close the closed-loop performance can approach the baseline open-loop result and what effect the yaw rate reference has on manoeuvre time.

5. Closed-loop control

The second objective of this study is to evaluate the relative performance of the yaw rate reference on manoeuvre time by including the closed-loop TV feedback controller in the system dynamics. This section describes the inclusion of the closed-loop TV controller in the system dynamics to achieve this objective and compares results considering permutations in yaw rate reference.

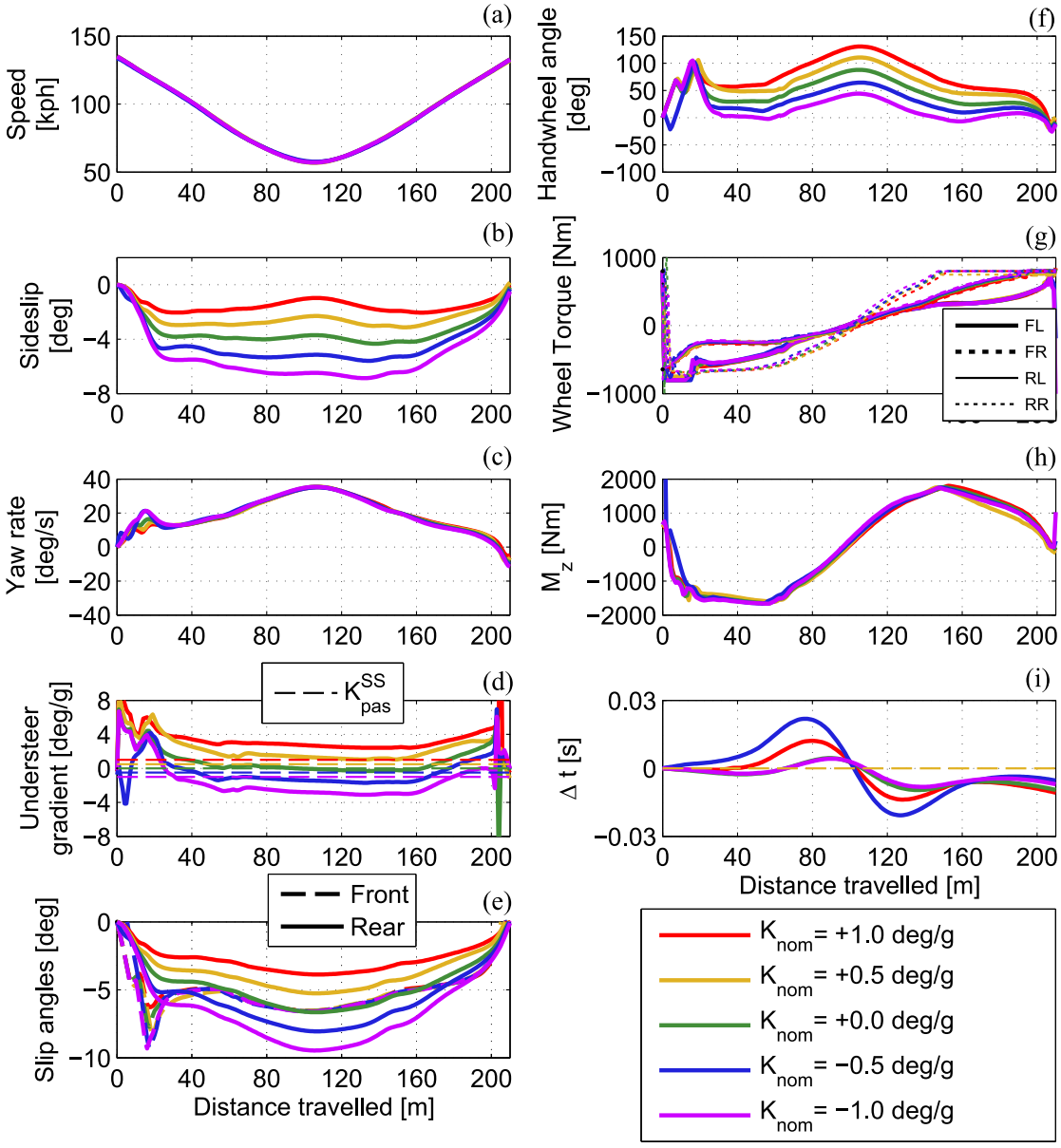

Figure 7.: Effect of varying passive understeer gradient (defined by steady-state cornering stiffness) on torque vectoring-controlled vehicle: states and controls

For optimisation of the closed-loop control algorithm (§3.1), modifications are made to the open-loop control method optimal control formulation used in §4. Figure 2(b) shows the optimal control configuration which including a simplified TV controller. The controller is composed of a yaw rate reference, which converts the driver steering angle input and vehicle speed into a reference yaw rate. Next, the controller takes the difference between the yaw rate reference and the vehicle yaw rate (yaw rate error) and applies a proportional gain to give one output: yaw moment demand, M_z. Finally, the control allocation determines the individual wheel torques, T_{ij}.

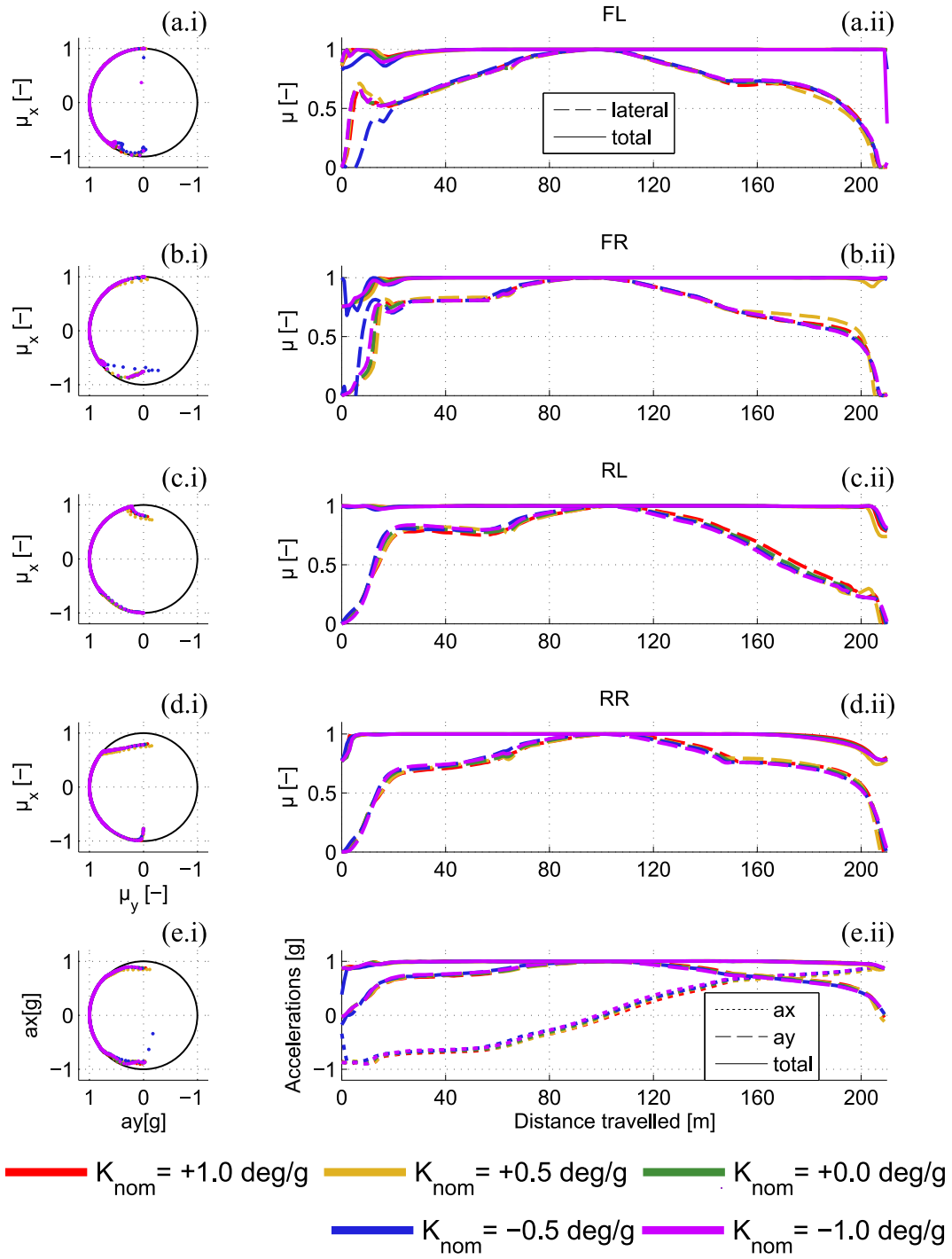

Figure 8.: Effect of varying passive understeer gradient (defined by steady-state cornering stiffness) on torque vectoring-controlled vehicle: friction utilisation

5.1. *Mathematical definition of TV controller in system dynamics*

The yaw rate reference, controller and CA are now incorporated into the mathematical definition of the system dynamics.

P controller

Feedback control is included in the form of a simple proportional-gain (P) controller:

$$M_z(s) = P\dot{\psi}_{err}(s), \tag{34}$$

where $\dot{\psi}_{err}$ is the yaw rate error.

To isolate the contribution of the yaw rate reference from the contribution of the performance of the system as a whole, it is important that the P controller is tuned in such a way as to deliver a consistent desired transient response. A parameter optimisation approach was used to find the P gain for a desired yaw response in the time domain. A single-track model was used as the plant, a step steer was applied with a constant forward speed and the yaw rate response simulated. The P gain was a decision variable chosen by Matlab function *fminsearchbnd* [40] such that the cost function minimised the root of the square of the yaw rate error between the desired yaw rate and actual yaw rate response. The desired transient yaw rate response, $\dot{\psi}_{ref}^{dyn}$, was generated as a first-order step response with 99% rise time, τ, of 0.2s chosen from experience in real-world data, rising to the steady-state value, $\dot{\psi}_{ref}^{SS}$, calculated from the steady-state yaw rate reference (42). The desired transient yaw rate response was:

$$\dot{\psi}_{ref}^{dyn} = \dot{\psi}_{ref}^{SS}(1 - e^{\frac{-t}{\tau}}) \tag{35}$$

This choice accords with Wong ([29], pp359) "*The optimum transient response of a vehicle is that which has the fastest response with a minimum of oscillation in the process of approaching the steady-state motion.*" The tuning process described was repeated for a range of speeds, and the mean value taken for the P gain, $P = 100\text{kNm/rads}^{-1}$ (to 1 significant figure).

Control Allocation

The requested yaw moment, M_z, is generated by the combination of wheel torques via the control allocation. After the overall difference in torque between the left and right tracks is calculated, the approach distributes torques front-rear by allocating wheel torques in proportion to the normal load on the axle, since this was found to be the optimal distribution in the literature for minimum time manoeuvring [13, 41] and in general permits a higher cornering force [1]. The following approach is simplified from [42].

First, torque limits are calculated for left and right tracks: the minimum of motor limits and adhesion limits. The achievable overall longitudinal torque, T_x, is converted to longitudinal force, F_x by dividing by the tyre radius. The torque that must be supplied by each track are given by the following equations:

$$T_L = \frac{r}{w}\left(\frac{w}{2}F_x - M_z\right), \tag{36}$$

$$T_R = \frac{r}{w}\left(\frac{w}{2}F_x + M_z\right), \tag{37}$$

$$\tag{38}$$

where T_L and T_R are the longitudinal torques to be supplied by the left and right tracks of the vehicle, respectively and w is the track width. The track torques are split front-rear

according to the proportion of normal load on each wheel:

$$T_{FL} = T_L \frac{f_{FLz}}{(f_{FLz} + f_{RLz})}, \qquad T_{FR} = T_R \frac{f_{FRz}}{(f_{FRz} + f_{RRz})}, \tag{39}$$

$$T_{RL} = T_L \frac{f_{RLz}}{(f_{FLz} + f_{RLz})}, \qquad T_{RR} = T_R \frac{f_{RRz}}{(f_{FRz} + f_{RRz})}. \tag{40}$$

$$\tag{41}$$

Thus, the overall torque demand, T_x, from the driver, and the yaw moment demand from the P-controller, M_z, are converted into the torques at each wheel, while considering motor and friction limits.

5.2. *Effect of target understeer gradient*

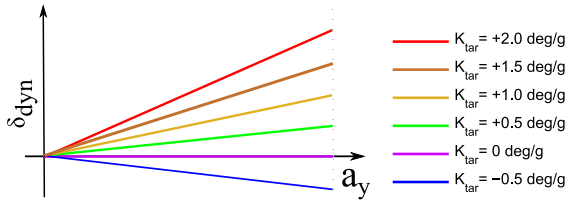

Figure 9.: The steady-state single-track yaw rate references parameterised by target understeer gradient, K_{tar}, expressed in 'handling diagram' form; dynamic steering angle against lateral acceleration.

It has been observed that the optimally-controlled open-loop *control method* (TV) can reduce manoeuvre time by 0.380s over the uncontrolled vehicle for a U-turn manoeuvre with radius $R = 35$m. Now, incorporating the feedback controller into the optimal control system dynamics, the effect of yaw rate reference will be evaluated.

The standard steady-state single-track yaw rate reference is of particular interest as it is the common reference adopted by the literature. It is defined [29]:

$$\dot{\psi}_{ref}^{SS} = \frac{V}{K_{tar} V^2 + L} \delta. \tag{42}$$

This is parameterised by the target understeer gradient, K_{tar}. The selection method of K_{tar} in the literature is heuristic, depending on preference for stability or agility. In this section, optimisations with $K_{tar} = \{-0.5, 0.0, +0.5, +1.0, +1.5, +2.0\}°/\text{g}$ are presented. These optimisations reveal: a) how close the causal *closed-loop control algorithm* can approach the a-causal baseline *open-loop control method*; b) the influence of target understeer gradient on manoeuvre time. Optimisations for a U-turn manoeuvre with $R = 35$m were run for each yaw rate reference. In Table 2, manoeuvre times and final time differences, Δt_f, relative to the open-loop (OL) baseline ($K_{pas}^{SS} = +0.5°/\text{g}$, penultimate column) and Δt_f to $K_{tar} = +0.5°/\text{g}$ (ultimate column) are set out. The closed-loop (CL) controller with $K_{tar} = +0.5°/\text{g}$ is able to complete the manoeuvre only +0.017s slower than the open-loop baseline. In the racing context, this could result in around +0.2s per 10-15 turn lap. The performance deficit of the closed-loop result to the baseline is 4% of the performance difference between *TV* and *Unctrl*, so a large proportion of the potential is realised.

Table 2.: Effect of yaw rate target (TV), Baseline $K_{pas}^{SS} = 0.5°/\text{g}$

Set-up	K_{tar} (°/g)	dev. from K_{pas}^{SS} (°/g)	Time (s)	Δt_f [a] (s)	Δt_f [b] (s)
OL	n/a	n/a	8.502	+0.000	-0.017
CL	2.0	+1.5	8.522	+0.019	+0.003
CL	1.5	+1.0	8.517	+0.015	-0.002
CL	1.0	+0.5	8.518	+0.016	-0.001
CL	+0.5	+0.0	8.519	+0.017	+0.000
CL	0.0	-0.5	8.523	+0.021	+0.005
CL	-0.5	-0.7	8.529	+0.027	+0.010

[a]Time difference with respect to open-loop baseline.

[b]Time difference with respect to $K_{tar} = K_{pas}^{SS} = +0.5°/\text{g}$.

The second purpose of this section was to evaluate the influence of target understeer gradient on performance using the single-track reference. Manoeuvre times for the single-track reference lie within 0.012s of each other, with a standard deviation of 0.004s. This is a very small variation, which cannot be reliably attributed to the system dynamics alone; discretisation and the particular numerical accuracies of the optimisation algorithm will have a bearing. Nevertheless, a physical explanation arising from the nonlinear tyre characteristics is given in §5.2.1. Thus, the data suggest that minimum time manoeuvring with TV is largely insensitive to target understeer gradient. Analysis of the vehicle behaviour over the course of the manoeuvre yields further insight. Figure 10 overlays states, controls and calculated quantities for the closed-loop optimisations: $K_{tar} = \{-0.5, 0, 0.5, 1.0, 2.0\}°/\text{g}$. Figure 10(a) shows a common speed trace for all cases. Of key interest is the yaw rate and understeer gradient, since these are the object of control and the high-level means by which to control it, respectively. Yaw rate (Figure 10(c)) follows the reference closely and, in so doing, achieves the target understeer gradient (Figure 10(d)) in all cases.

Sideslip (Figure 10(b)) is tail-out for all simulations, with increasing magnitude as understeer gradient reduces. The difference in sideslip between most extreme targets ($K_{tar} = 2°/\text{g}$ and $K_{tar} = -0.5°/\text{g}$) has a maximum over the course of the manoeuvre of 2.5°. The maximum difference between optimisations of handwheel angle is 40°, which is a significant difference in workload for the driver.

The most noteworthy feature of these results is that a very similar yaw rate is achieved for each understeer target. There is, therefore, a general yaw rate profile for this particular K_{pas}^{SS}, that minimises manoeuvre time to within a very small tolerance—yet it is achieved through a variety of combinations of target understeer gradients and driver control inputs. According to equation (42), the only means to achieve the same yaw rate profile is by modification of the steering angle, as L and K_{tar} are constant and V is to be maximised at all times and does not vary according to target. Figure 10(f) shows that handwheel angle is increased in inverse proportion to K_{tar}, with greatest steering angles required for $K_{tar} = 2°/\text{g}$. Note that the ability to follow this yaw rate profile is dependent on the 'perfect' driver (which the optimal control represents) to maximise the potential of the controlled-vehicle set-up.

The yaw moment provided by the torque difference between left and right tracks shows a similar trend for all targets: stabilising effect during braking and destabilising during acceleration. A greater magnitude of yaw moment (and therefore torque difference across tracks) is required as understeer target decreases, observable in the regions $20 < s < 60$m

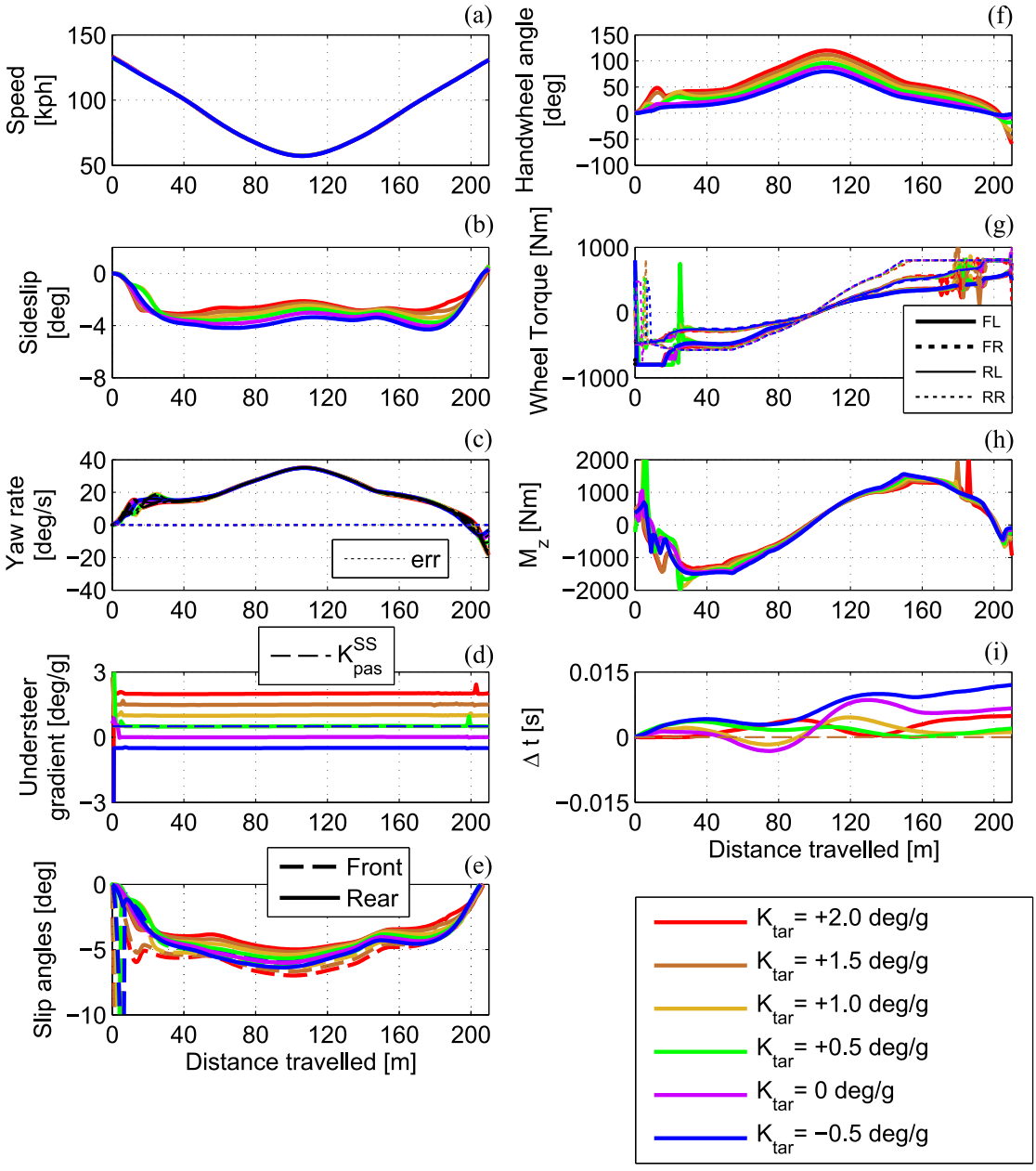

Figure 10.: Comparison of closed-loop torque vectoring performance for a range of over-steering to understeering target gradients, K_{tar}: states and controls.

and $120 < s < 180$m.

Further insight is drawn from plots of friction utilisation, as shown in Figure 11. The immediate observation is that, with the exception of the initial and final 10m and 20m respectively where torque is limited, friction utilisation is maximal for every tyre, for every understeer target. Maximum total friction use is key to maximum performance. This is a combination of the effects of torque vectoring and driver control inputs.

The steady-state single-track reference is a simple expression, parameterised by the length of the vehicle in addition to the understeer target. This simplicity is undoubtedly a key reason for its widespread adoption in the literature.

Results of the open-loop control method optimisations in §4 demonstrated that torque

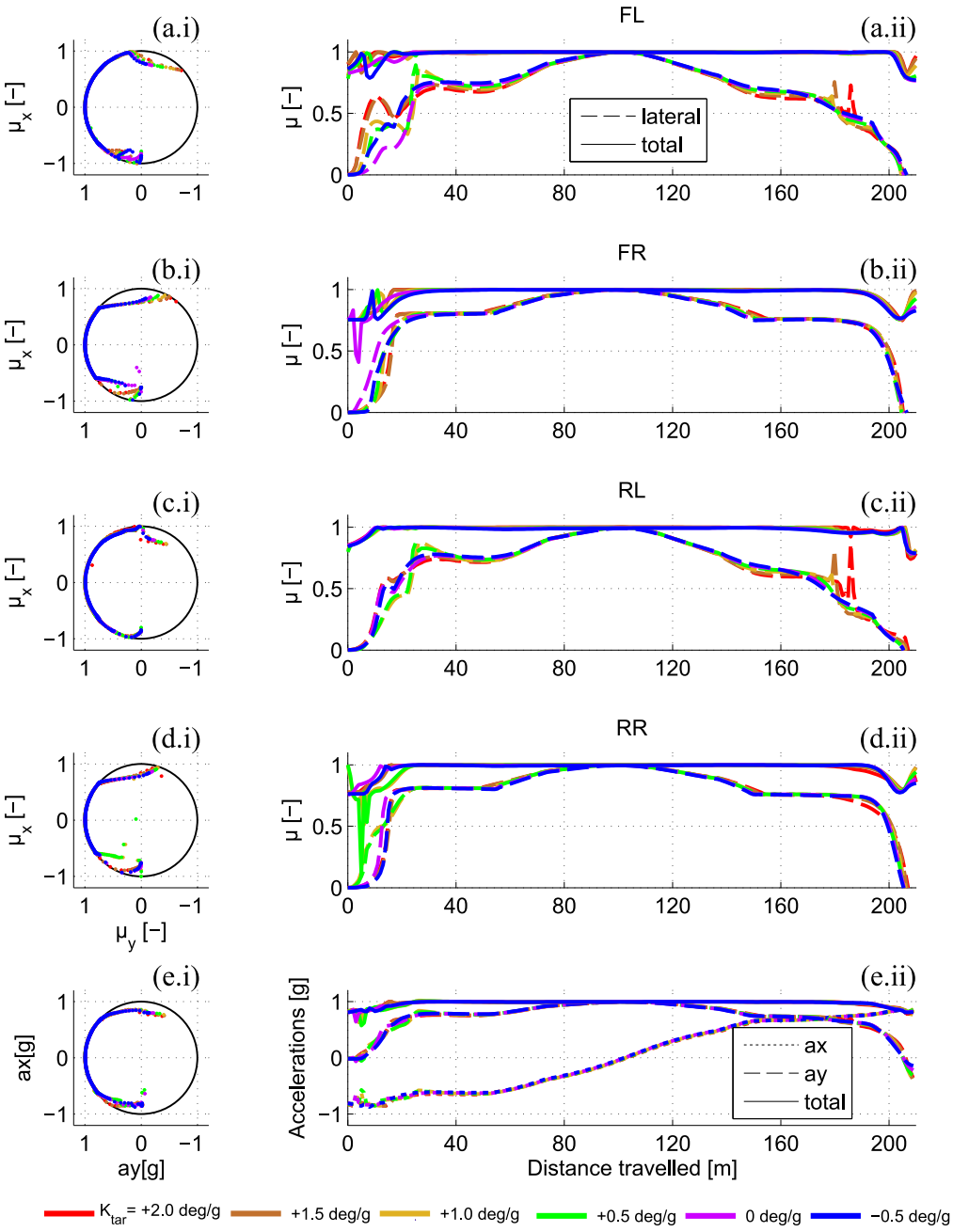

Figure 11.: Comparison of closed-loop torque vectoring performance for a range of oversteering to understeering target gradients, K_{tar}: friction utilisation

vectoring seeks to neutralise the negative effects of weight transfer on total cornering force. It achieves this using two mechanisms: directly by generating a yaw moment from the left-right torque difference; indirectly by longitudinal forces influencing the cornering stiffness and therefore lateral forces (and the associated yaw moments generated) through coupling effects. In effect, the steady-state single track reference commands not only no lateral load transfer (since there is no track width) but also no longitudinal load transfer (since it does not consider longitudinal dynamics). Thus, its inherent characteristics match the characteristics observed in the optimal baseline open-loop results, and this is why it delivers a very high level of performance even in the 7DOF model.

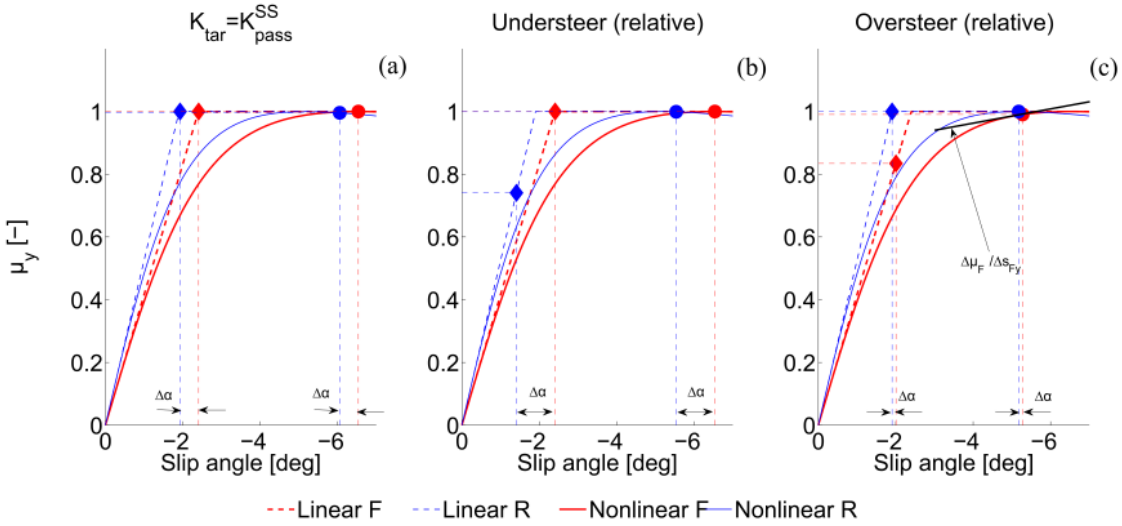

Figure 12.: Linear and nonlinear lateral tyre friction curves for steady-state cornering as a function of slip angle. Operating points shown following understeer gradient targets (a) where $K_{tar} = K_{pas}^{SS}$, (b) relative understeer with respect to K_{pas}^{SS}, and (c) relative oversteer with respect to K_{pas}^{SS}.

In this section, it has been demonstrated that in spite of the simplicity of the single-track yaw rate reference, a high level of performance is still achieved. This level of performance is not affected by the choice of target understeer gradient, opening up the possibility of selecting the target based on driver preference, without loss of performance.

5.2.1. Effect of tyre model

In previous work by the authors [22], a similar methodology was followed with a lower-order, 3DOF single-track model with linear tyre forces constrained by front and rear friction circles, longitudinal dynamics including longitudinal load transfer and TV emulated by an externally-applied yaw moment. In contradiction to the 7DOF model findings presented in this section, for the 3DOF model it was found that, for the closed-loop optimisations, manoeuvre time was minimised by setting $K_{tar} = K_{pas}^{SS}$ and significant degradation in time was found when K_{tar} deviated from K_{pas}^{SS}. This phenomenon can be explained by studying the tyre friction curves as a function of slip. For simplicity, Figure 12 plots lateral friction against slip angle, assuming pure steady state cornering with zero longitudinal acceleration. Linear and nonlinear tyre models are shown for front and rear tyres. Rear stiffness is greater than front stiffness to give $K_{pas}^{SS} = 0.5°/\text{g}$. The tyre models are equivalent at zero slip only ($\eta_i = B_i C D$) and hence the nonlinear tyre lags the linear at higher values of slip, and reaches its peak at a higher slip angle.

To achieve a target understeer gradient at a given lateral acceleration, a difference in slip angles, $\Delta\alpha$, is required, since understeer gradient is related to slip angles from the definition [29] (note that this is equivalent to equation 32):

$$K_{SS} = (|\alpha_f| - |\alpha_r|)/a_y = \Delta\alpha/a_y. \tag{43}$$

To demonstrate and explain the difference between the tyre models, reference are made to the three cases of $K_{tar} = K_{pas}^{SS}$, as well as understeer and oversteer targets in Figure 12(a), (b) and (c) respectively.

- **Target=Passive.** $K_{tar} = K_{pas}^{SS}$ (Figure 12(a)). As steady-state velocity is increased, lateral acceleration and slip angles increase. The peak tyre friction is approached at front and rear simultaneously for the linear tyre, since $\Delta\alpha$ to respect the K_{tar} matches that for K_{pas}^{SS}. Total tyre friction is $\sum \mu = 2$. For the nonlinear tyre, the cornering stiffness is not identical front and rear, at high slip angles, so peak tyre friction is reached at front slightly before rear, but still offering near-maximal total friction ($\sum \mu_{nonlinear} \sim 2$).
- **Relative understeer:** $K_{tar} > K_{pas}^{SS}$(Figure 12(b)). In this case, the front tyres peak first: a greater $\Delta\alpha$ is required than for K_{pas}^{SS}, and hence for the linear case, the rear tyres cannot deliver maximum friction utilisation ($\sum \mu \sim 1.75$). For the nonlinear tyres, the same $\Delta\alpha$ is required, yet $\sum \mu_{nonlinear} \sim 2$. As slip angle increases and the peak of the $\mu-$slip curve is approached, the gradient of the curve for the linear tyre remains high, whereas in the nonlinear case the gradient approaches zero.
- **Relative oversteer:** $K_{tar} < K_{pas}^{SS}$(Figure 12(c)). This is a similar situation to relative understeer, except that the rear tyres saturate first. $\Delta\alpha$ is much smaller than for K_{pas}^{SS} (and is still positive, since in absolute terms, the target is still mildly understeering). For the linear case, the front tyres cannot deliver maximum friction utilisation ($\sum \mu \sim 1.82$). Again, the $\Delta\mu/\Delta\alpha$ gradient at the peak of the nonlinear tyres is close to zero for the rear tyre. However, the front tyre is operating further from the peak that in (a) and (b) and hence the the $\Delta\mu_F/\Delta s_{Fy}$ gradient is slightly increased — yet the total tyre friction generated is still close to maximal.

Therefore, at any target where $K_{tar} \neq K_{pas}^{SS}$, tyre friction levels for linear are non-maximum (decreasing as the difference between the target and the passive increases) whereas the nonlinear tyre model is always close to maximal, since even with a large difference in slip angles (front-rear), the reduction in tyre friction will be very small. Tyre force coupling of the nonlinear tyres below the limit further improves the overall friction level, as at high slip ratios, the $\Delta\mu/\Delta\alpha$ angle gradients are even closer to zero as the peak is approached. Further investigation revealed that lateral load transfer contributes a minor influence but the control allocation distributing torque according to normal load ensures that tyre cornering stiffnesses are equalised as far as possible between all four tyres.

Remark 3 Clearly, if a sufficiently large $\Delta\alpha$ was imposed by the TV controller, nonlinear tyres would result in loss of $\sum \mu_{nonlinear}$. However, for the range of K_{tar} considered in this paper (resulting in large variation in maximum steering angle) the optimal performance is practically insensitive to K_{tar}.

6. Conclusions

This work has studied the effect of handling characteristics, passively and actively modified, of torque-vectored vehicles for minimum time manoeuvring. Optimal control techniques were used to generate open-loop control trajectories for a U-turn manoeuvre for an electric vehicle with four independent motors. Results confirmed that TV is able to compensate for adverse load transfer effects encountered during acceleration, braking and high lateral accelerations. The effect of altering the passive handling of the vehicle was studied, concluding that, while the passive characteristics of the vehicle had negligible effect on the minimum time performance of the TV-controlled vehicle, notable differences in the steering input and sideslip response were observed.

An optimal control framework that incorporated a TV controller in the system dynamics was then used to evaluate the ability of the controller to realise the baseline potential when following a yaw rate reference. The standard steady-state single-track model reference was shown to come close to the baseline performance. Finally, a major finding of this work demonstrated that manoeuvre time for the reference-following TV vehicle is largely insensitive to target understeer gradient, opening up the possibility of subjective target selection without compromising performance. It was shown that this insensitivity is attributable to tyre nonlinearity.

Acknowledgements

A.M.D.G.
For support with optimal control, Efstathios Siampis.

Disclosure Statement

No potential conflict of interest was reported by the authors.

Funding

This work was supported by the Engineering and Physical Sciences Research Council Industrial Cooperative Awards in Science & Technology studentship with sponsor Jaguar Land Rover under Grant EP/K504324/1.

References

[1] Shibahata Y, Shimada K, Tomari T. Improvement of vehicle manoeuvrability by direct yaw moment control. Vehicle System Dynamics. 1993;22(5-6):465–481.
[2] Shimada K, Shibahata Y. Comparison of three active chassis control methods for stabilizing yaw moments. SAE Technical Paper; 1994.
[3] Bedner E, Fulk D, Hac A. Exploring the trade-off of handling stability and responsiveness with advanced control systems. SAE Papers. 2007;:01–0812.
[4] Van Zanten AT. Bosch ESP Systems: 5 Years of Experience. Warrendale, PA: SAE International; 2000. SAE Technical Paper 2000-01-1633.
[5] Manning W, Crolla D. A review of yaw rate and sideslip controllers for passenger vehicles. Transactions of the Institute of Measurement and Control. 2007;29(2):117–135.
[6] Sawase K, Ushiroda Y, Inoue K. Effect of the right-and-left torque vectoring system in various types of drivetrain. SAE Technical Paper; 2007.
[7] Crolla DA, Cao D. The impact of hybrid and electric powertrains on vehicle dynamics, control systems and energy regeneration. Vehicle System Dynamics. 2010 Jan;50(sup1):95–109.
[8] Jonasson M, Andreasson J, Jacobson B,Trigell AS. Global force potential of over-actuated vehicles. Vehicle System Dynamics. 2010 Jan;48(9):983–998.
[9] De Novellis L, Sorniotti A, Gruber P. Wheel torque distribution criteria for electric vehicles with torque-vectoring differentials. IEEE transactions on vehicular technology. 2014;63(4):1593–1602.
[10] Siampis E, Velenis E, Longo S. Rear wheel torque vectoring model predictive control with velocity regulation for electric vehicles. VSD. 2015;53(11):1555–1579.
[11] Kaiser G, Liu Q, Hoffmann C, Korte M, Werner H. Torque vectoring for an electric vehicle using an LPV drive controller and a torque and slip limiter. In: Decision and Control (CDC), 2012 IEEE 51st Annual Conference on. IEEE; 2012. p. 5016–5021.

[12] De Novellis L, Sorniotti A, Gruber P, Orus J, Rodriguez Fortun JM, Theunissen J, De Smet J. Direct yaw moment control actuated through electric drivetrains and friction brakes: Theoretical design and experimental assessment. Mechatronics. 2015 Mar;26:1–15.
[13] de Castro R, Tanelli M, Araujo RE, Savaresi SM. Minimum-time manoeuvring in electric vehicles with four wheel-individual-motors. VSD. 2014 Jun;52(6):824–846.
[14] Casanova D, Sharp R, Symonds P. Minimum time manoeuvring: The significance of yaw inertia. Vehicle System Dynamics. 2000;34(2):77–115.
[15] Casanova D. On minimum time vehicle manoeuvring: The theoretical optimal lap. PhD Thesis. Cranfield Univesity 2000.
[16] Brayshaw D. Use of numerical optimisation to determine on-limit handling behaviour of race cars. PhD Thesis. Cranfield Univesity 2004.
[17] Perantoni G, Limebeer DJ. Optimal control for a formula one car with variable parameters. Vehicle System Dynamics. 2014;52(5):653–678.
[18] Tremlett A, Massaro M, Purdy D, Velenis E, Assadian F, Moore A, Halley M. Optimal control of motorsport differentials. Vehicle System Dynamics. 2015;53(12):1772–1794.
[19] Velenis E, Tsiotras P, Lu J. Optimality properties and driver input parameterization for trail-braking cornering. European Journal of Control. 2008;14(4):308–320.
[20] Tavernini D, Massaro M, Velenis E, Katzourakis DI, Lot R. Minimum time cornering: the effect of road surface and car transmission layout. Vehicle System Dynamics. 2013 Oct;51(10):1533–1547.
[21] Smith E, Tavernini D, Claret C, Velenis E, Cao D. Optimal yaw-rate target for electric vehicle torque vectoring system. In: The Dynamics of Vehicles on Roads and Tracks: Proceedings of the 24th Symposium of the International Association for Vehicle System Dynamics (IAVSD 2015), Graz, Austria, 17-21 August 2015. CRC Press; 2016. p. 107.
[22] Smith E, Velenis E, Cao D, Tavernini D. Evaluation of optimal yaw rate reference for electric vehicle torque vectoring. In: Advanced Vehicle Control: Proceedings of the 13th International Symposium on Advanced Vehicle Control (AVEC'16), September 13-16, 2016, Munich, Germany; Dec. CRC Press/Balkema; 2016. p. 619–624; Available from: http://dx.doi.org/10.1201/9781315265285-98.
[23] Tremlett A, Assadian F, Purdy D, Vaughan N, Moore A, Halley M. Quasi-steady-state linearisation of the racing vehicle acceleration envelope: a limited slip differential example. Vehicle System Dynamics. 2014;52(11):1416–1442.
[24] Horiuchi S. Evaluation of chassis control method through optimisation-based controllability region computation. Vehicle System Dynamics. 2012;50(sup1):19–31.
[25] Horiuchi S. Evaluation of chassis control algorithms using controllability region analysis. In: The Dynamics of Vehicles on Roads and Tracks: Proceedings of the 24th Symposium of the International Association for Vehicle System Dynamics (IAVSD 2015), Graz, Austria, 17-21 August 2015. CRC Press; 2016. p. 35.
[26] Levin JM, Nahon M, Paranjape AA. Aggressive turn-around manoeuvres with an agile fixed-wing UAV. IFAC-PapersOnLine. 2016;49(17):242–247.
[27] Bakker E, Nyborg L, Pacejka HB. Tyre modelling for use in vehicle dynamics studies. SAE Technical Paper; 1987.
[28] Velenis E, Katzourakis D, Frazzoli E, Tsiotras P, Happee R. Steady-state drifting stabilization of rwd vehicles. Control Engineering Practice. 2011;19(11):1363–1376.
[29] Wong JY. Theory of ground vehicles. John Wiley & Sons; 2001.
[30] Milliken WF, Milliken DL. Race car vehicle dynamics. Vol. 400. Society of Automotive Engineers Warrendale; 1995.
[31] Cossalter V, Da Lio M, Lot R, Fabbri L. A general method for the evaluation of vehicle manoeuvrability with special emphasis on motorcycles. Vehicle system dynamics. 1999;31(2):113–135.
[32] Yuhara N, Tajima J. Advanced steering system adaptable to lateral control task and driver's intention. Vehicle System Dynamics. 2001;36(2-3):119–158.
[33] Massaro M, Cole D. Neuromuscular-steering dynamics: Motorcycle riders vs. car drivers. In: ASME 2012 5th Annual Dynamic Systems and Control Conference joint with the JSME 2012 11th Motion and Vibration Conference. American Society of Mechanical Engineers; 2012. p. 217–224.
[34] Patterson MA, Rao AV. GPOPS-II: A MATLAB software for solving multiple-phase optimal control problems using hp–adaptive gaussian quadrature collocation methods and sparse nonlinear programming. ACM TOMS. 2013;39(3):1–41.
[35] Weinstein MJ, Rao AV. A source transformation via operator overloading method for the automatic differentiation of mathematical functions in matlab. ACM Transactions on Mathematical Software (TOMS). 2016;42(2):11.
[36] Betts JT. Practical methods for optimal control and estimation using nonlinear programming.

Vol. 19. Siam; 2001.
[37] Limebeer D, Perantoni G. Optimal control of a formula one car on a three-dimensional trackpart 2: Optimal control. Journal of Dynamic Systems, Measurement, and Control. 2015;137(5):051019.
[38] Tremlett A, Assadian F, Purdy D, Vaughan N, Moore A, Halley M. The control authority of passive and active torque vectoring differentials for motorsport applications. In: Proceedings of the FISITA 2012 World Automotive Congress. Springer; 2013. p. 335–347.
[39] Kaspar S, Pruckner A, Stroph R, Hohmann S. Potential of vehicle dynamics via single wheel drive for installation space optimized electric vehicles. In: Aachener Kolloquium Fahrzeug-und Motorentechnik, Aachen; 2012.
[40] Senn M. fminsearchbnd, fminsearchcon - File Exchange - MATLAB Central. 2012 (accessed January 25, 2017); Available from: `http://uk.mathworks.com/matlabcentral/fileexchange/8277-fminsearchbnd--fminsearchcon`.
[41] Pennycott A, De Novellis L, Sorniotti A, Gruber P. The Application of Control and Wheel Torque Allocation Techniques to Driving Modes for Fully Electric Vehicles. Warrendale, PA: SAE International; 2014. Report No.: 2014-01-0085.
[42] Claret C. Torque vectoring control for electric and brake-by-wire vehicles: Masters thesis. Cranfield University; 2014.